THE TRANSIT LIGHT CURVE PROJECT. I. FOUR CONSECUTIVE TRANSITS OF THE EXOPLANET XO-1b

Matthew J. Holman,[1] Joshua N. Winn,[2] David W. Latham,[1] Francis T. O'Donovan,[3] David Charbonneau,[1,4]
Gáspár A. Bakos,[1,5] Gilbert A. Esquerdo,[1,6] Carl Hergenrother,[1,7] Mark E. Everett,[6] and András Pál[1,8]

ABSTRACT

We present *RIz* photometry of four consecutive transits of the newly discovered exoplanet XO-1b. We improve on the estimates of the transit parameters, finding the planetary radius to be $R_P = 1.184^{+0.028}_{-0.018} R_J$, and the stellar radius to be $R_\star = 0.928^{+0.018}_{-0.013} R_\odot$, assuming a stellar mass of $M_\star = (1.00 \pm 0.03) \, M_\odot$. The uncertainties in the planetary and stellar radii are dominated by the uncertainty in the stellar mass. These uncertainties increase by a factor of 2–3 if a more conservative uncertainty of 0.10 $M_\odot$ is assumed for the stellar mass. Our estimate of the planetary radius is smaller than that reported by McCullough and coworkers, and the resulting estimate for the mean density of XO-1b is intermediate between that of the low-density planet HD 209458b and the higher density planets TrES-1 and HD 189733b. The timings of the transits have an accuracy ranging from 0.2 to 2.5 minutes and are marginally consistent with a uniform period.

Subject headings: planetary systems — stars: individual (GSC 02041-01657) — techniques: photometric

Online material: machine-readable table

1. INTRODUCTION

An exoplanetary transit is a rare opportunity to learn a great deal about both the planet and the star. With precise measurements of the amount of light blocked by the planet as a function of time, it is possible to infer the relative sizes of the star and planet, the orbital inclination, and the stellar limb-darkening function. Coupled with measurements of the time-variable Doppler shift of the star and an estimate of the stellar mass, one learns the planetary mass and the stellar radius. These fundamental measurements set the stage for a host of more subtle measurements of effects such as planetary atmospheric absorption lines, thermal emission, spin-orbit alignment, and timing anomalies, as reviewed recently by Charbonneau et al. (2006a).

For these reasons, newly discovered transiting exoplanets are welcomed with open arms. The tenth such object was recently reported by McCullough et al. (2006). The parent star, XO-1, is bright ($V = 11$; G1 V), making it a favorable target for precise observations. The planet has an orbital period of ~4 days and a mass and radius comparable to Jupiter, although McCullough et al. (2006) pointed out that their photometry actually implies a mean density that is somewhat smaller than theoretical expectations for "hot Jupiters." If confirmed, this would put XO-1b in the same category as the anomalously large planet HD 209458b, and may have implications for the various theories that have been espoused for that object.

Two of us (M. J. H. and J. N. W.) have initiated the Transit Light Curve (TLC) Project, a long-term campaign to build a library of high-precision transit photometry, with the dual goals of (1) refining the estimates of the physical and orbital parameters of the target systems, and (2) searching for secular and short-term variations in the transit times (and light curves) that would be indicative of perturbations from additional bodies (Agol et al. 2005; Holman & Murray 2005). Here, we present results for XO-1b that were obtained as part of this program. We describe the observations and the data reduction procedures in § 2. In § 3 we describe the model and techniques we used to estimate the physical and orbital parameters of the XO-1 system, and in § 4 we summarize our results.

2. THE OBSERVATIONS AND DATA REDUCTION

We observed four consecutive transits of XO-1b. According to the ephemeris provided by McCullough et al. (2006),

$$T_c(E) = 2,453,808.9170(\text{HJD}) + E(3.941534 \text{ days}), \quad (1)$$

these transits correspond to epochs 17–20. We employed three different telescopes: the Fred L. Whipple Observatory (FLWO) 1.2 m telescope (for $E = 19, 20$), the Palomar 1.5 m telescope (for $E = 17$), and the TopHAT 0.26 m telescope (for $E = 17, 18, 19$).

2.1. *FLWO* 1.2 m *z Photometry*

We observed the $E = 19, 20$ transits (UT 2006 May 28 and June 1) with KeplerCam on the 1.2 m (48 inch) telescope of the FLWO on Mt. Hopkins, Arizona. This camera (PI: D. Latham) was built for a photometric survey of the target field of the *Kepler* satellite mission (Borucki et al. 2003). It has a single $4K \times 4K$ Fairchild 486 CCD with a $23'.1 \times 23'.1$ field of view. We used 2×2 binning, for which the readout and reset time is 11.5 s and the typical read noise is 7 e^- per binned pixel. The response of each amplifier deviates from linearity by less than 0.5% over the range of counts from the faintest to brightest comparison star. We observed through the Sloan Digital Sky Survey (SDSS) *z* filter, the reddest available band, in order to minimize the effects of limb-darkening and color-dependent atmospheric extinction. The effective bandpass at the red end

[1] Harvard-Smithsonian Center for Astrophysics, 60 Garden Street, Cambridge, MA 02138; mholman@cfa.harvard.edu.
[2] Department of Physics, and Kavli Institute for Astrophysics and Space Research, Massachusetts Institute of Technology, Cambridge, MA 02139.
[3] California Institute of Technology, 1200 East California Boulevard, Pasadena, CA 91125.
[4] Alfred P. Sloan Research Fellow.
[5] Hubble Fellow.
[6] Planetary Science Institute, 1700 East Fort Lowell, Tucson, AZ 85719.
[7] Also at: Lunar and Planetary Laboratory, University of Arizona, Tucson, AZ 85719.
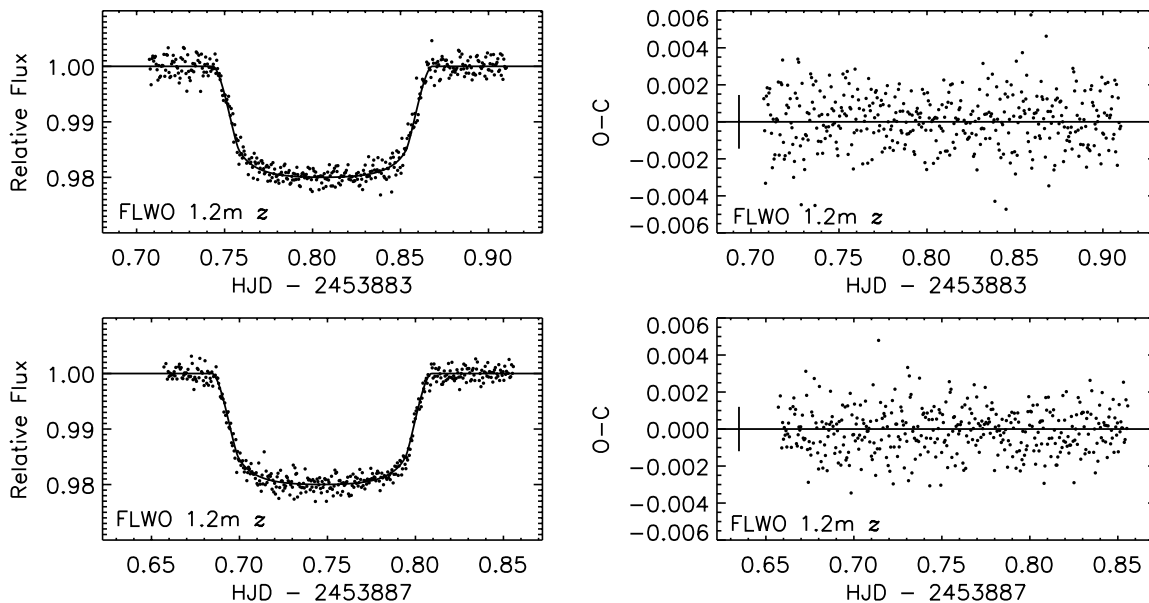[8] Also at: Eötvös Loránd University, Budapest, Hungary.

Fig. 1.—Relative *z*-band photometry of XO-1. The left panels show the photometry (*points*) and the best-fitting model (*solid line*). The right panels show the residuals (observed/calculated) and representative 1 σ error bars that have been rescaled such that the χ^2 per degree of freedom for each time series is unity. For the first transit ($E = 19$), the rms residual is 0.15%. For the second transit, the rms residual is 0.12%.

was limited by the quantum efficiency of the CCD, which drops from ~100% at 7500 Å to ~10% at 10500 Å. We defocused the telescope slightly in order to enhance the duty cycle and average over pixel-to-pixel sensitivity variations. The full width at half-maximum (FWHM) of a stellar image was typically ~3 binned pixels (2″). We used automatic guiding to maintain the locations of XO-1 and its comparison stars to within a few pixels over the course of both nights. On each night, we repeatedly took 30 s exposures for approximately 5 hr bracketing the predicted transit midpoint. The conditions on UT 2006 May 28 appeared photometric, and the images were taken through air masses ranging from 1.00 to 1.22. The conditions on UT 2006 June 1 were nearly photometric, except for very thin, high clouds that passed through the field between UT 5:50 and 6:30. The air mass range on this night was from 1.00 to 1.31.

The images were calibrated using standard IRAF[9] procedures for the overscan correction, trimming, bias subtraction, and flat-field division. We did not attempt to correct the fringing that was apparent with the *z* filter. The fringing had a small amplitude and little effect on the final photometry, given the accuracy of the automatic guiding. We excluded three images the first night that showed significant large-scale features that were not corrected by the flat field (presumably from clouds), and one from the second night that was contaminated by an artificial satellite trail. We then performed aperture photometry of XO-1 and four nearby stars of comparable brightness and color (stars 1, 3, 6, and 7 from Table 1 of McCullough et al. 2006), using an aperture radius of 6.5 pixels (4″3) for both nights. We subtracted the underlying contribution from the sky, after estimating its brightness within an annulus ranging from 30 to 35 pixels in radius, centered on each star. We divided the flux of XO-1 by the total flux of the comparison stars. We then fit a linear function of time to the pre-ingress and post-egress data and divided the entire time series by this function, in order to normalize the

flux and remove residual systematic effects. A function of time proved to be a slightly better fit than the more traditional function of air mass.

To estimate the uncertainties in our photometry, we computed the quadrature sum of the errors due to Poisson noise of the stars (both XO-1 and the comparison stars), Poisson noise of the sky background, readout noise, and scintillation noise (as estimated according to the empirical formulas of Young [1967] and Dravins et al. [1998]). The dominant term is the Poisson noise from XO-1. The final time series is plotted in Figure 1 and is available in electronic form in Table 1.

2.2. *TopHAT I Photometry*

We used TopHAT to observe the $E = 17, 18, 19$ transits of XO-1b (UT 2006 May 20, 24, and 28). TopHAT is an automated telescope, also located on Mt. Hopkins, Arizona, which was designed for photometric follow-up observations of transiting exoplanet candidates identified by the HAT network (Bakos et al. 2004). It consists of a 0.26 m diameter f/5 commercially available Baker Ritchey-Chrétien telescope on an equatorial fork mount. A 1°.25 square field of view is imaged onto a 2K × 2K Peltier-cooled, thinned CCD detector, yielding a pixel scale of 2″.2. In order to extend the integration times and increase the duty cycle of the observations, we applied a slight

TABLE 1
PHOTOMETRY OF XO-1

Telescope	Filter	HJD	Relative Flux	Uncertainty
FLWO 48 inch.........	*z*	2,453,883.70727	1.00125	0.00147
Palomar 60 inch.......	*R*	2,453,875.77023	1.00144	0.00215
TopHAT...................	*I*	2,453,875.64414	1.00889	0.00386

NOTES.—Table 1 is published in its entirety in the electronic edition of the *Astrophysical Journal*. A portion is shown here for guidance regarding its form and content. The data are also available in digital form from the authors on request. The time stamps represent the Heliocentric Julian Date at the time of midexposure. The uncertainty estimates are based on the procedures described in § 2.

---

[9] IRAF is distributed by the National Optical Astronomy Observatories, which are operated by the Association of Universities for Research in Astronomy, Inc., under cooperative agreement with the National Science Foundation.
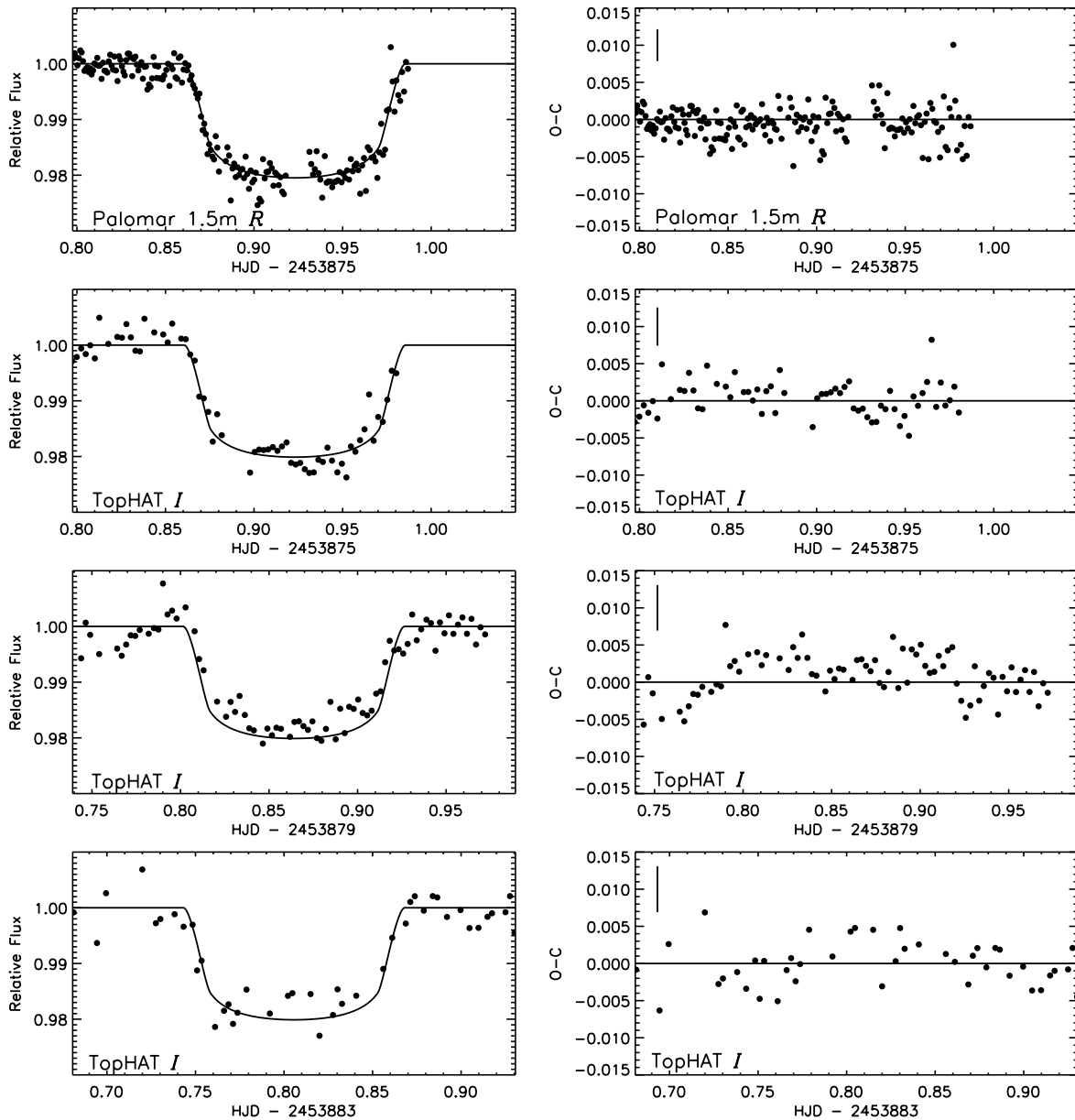
FIG. 2.—Relative *R*- and *I*-band photometry of XO-1. The left panels show the photometry (*points*) and the best-fitting model (*solid line*). The right panels show the residuals (observed/calculated) and representative 1 σ error bars, estimated as described in the text. From top to bottom, the rms residuals are 0.21%, 0.28%, 0.31%, and 0.32%.

defocusing. The resulting point-spread function (PSF) had a FWHM of 2.1 pixels (4.″6). On each night, we observed for approximately 5 hr.

We calibrated the images by subtracting the overscan bias and a scaled dark image and dividing by an average sky flat from which large outliers had been rejected. We performed aperture photometry on XO-1 and on an additional ~800 stars in the field, using an aperture of radius 5 pixels (11.″0) and an exterior annulus for sky subtraction. Most of the 800 stars (after removing variables) were used as calibrators in a statistically weighted manner to transform the magnitudes of the individual frames to the instrumental magnitude system of a selected reference frame. The derived light curve still suffers from small-amplitude systematic errors. In order to minimize them, we used all the out-of-transit data (assuming them to be of constant brightness) to find the correlation with the air mass, hour angle (linear fits), pixel position (sinusoidal function), and Gaussian profile parameters (second-order fits). The fitted function was then applied to and subtracted

from the entire light curve, including the transits. These corrections in this postprocessing step were of the order of 3 mmag or less for unsaturated points. The resulting time series is shown in Figure 2 and listed in Table 1, along with the Palomar data described below.

2.3. *Palomar* 1.5 m *R Photometry*

We observed the $E = 17$ transit with the 1.5 m (60 inch) telescope at Palomar Observatory. The CCD camera has $2K \times 2K$ pixels with a plate scale of 0.″378 pixel^{-1}. In order to increase the duty cycle, we read out only half of the available field of view, yielding an effective field size of 12.′9 × 6.′5. The sky was cloud-free, the typical seeing was 1.″5, and the observations ranged in air mass from 1.01 to 1.45. We gathered 209 *R*-band images spanning 5.2 hr, with integration times of 20 s and a cadence that increased from 65 to 90 s over the course of the observing sequence. The observing sequence was briefly interrupted twice (once prior to ingress, and once near midtransit) by

telescope calibration scripts that are required as part of its robotic operation.

We used the automated P60 reduction pipeline to calibrate the images. This pipeline trims the overscan columns, subtracts the bias level, divides by a dome flat, and flags bad pixels. We performed aperture photometry of XO-1 and five comparison stars, using an aperture of radius 9 pixels (3″4) and an annulus for sky subtraction ranging in radius from 30 to 45 pixels. We divided the flux of XO-1 by the sum of the fluxes of the comparison stars and normalized the resulting time series to produce a flux of unity in the pre-ingress data. The rms variation of the pre-ingress data is 0.17%, which we adopted as the photometric uncertainty in each data point. The pointing drifted by as much as 35 pixels (13″) during the course of the observations. We believe that this drift, coupled with uncertainties in the flat-field image, is responsible for the poorer quality of the Palomar 1.5 m data compared to those from the FLWO 1.2 m. The Palomar data are presented in Figure 2 and listed in Table 1.

3. THE MODEL

The planetary, stellar, and orbital parameters were inferred by fitting a parameterized model to all of the photometry simultaneously. The model is based on a star and a planet on a circular orbit about their center of mass.[10] The star has a mass $M_\star$ and radius $R_\star$, and the planet has a mass M_P and radius R_P. The orbit has a period P and an inclination i relative to the sky plane. We define the coordinate system such that $0° \le i \le 90°$. The initial condition is specified by T_c, a particular time of conjunction (the transit midpoint). When the planet is projected in front of the star, the model flux declines by an amount that depends on the projected separation, on the stellar limb-darkening function, and also on the planet-to-star area ratio. To compute this flux decrement, we assume a quadratic limb-darkening law and employ the analytic formulas of Mandel & Agol (2002). The R- and I-band data are not of sufficiently high signal-to-noise ratio to justify this treatment; instead, we fix combinations of both the R and I limb-darkening parameters at the values estimated by Claret (2000) for a star of the observed effective temperature, surface gravity, and metallicity (see Table 5 of McCullough et al. 2006).

We allow the T_c for each of the four transits to be an independent parameter. This is because we seek to measure or bound any timing anomalies that may indicate the presence of moons or additional planets in the system. Obviously, if we allow each of the four T_c values to vary, we cannot independently determine the orbital period. Instead, we fix $P = 3.941534$ days, the value reported by McCullough et al. (2006). This mean period is based on observations spanning a few years and is known more accurately than we could hope to determine from our time baseline of 12 days. The quoted uncertainty in the mean period is only 0.000027 days and is negligible for our purposes.

There is a well-known degeneracy among $M_\star$, $R_\star$, and R_P that prevents all three parameters from being uniquely determined from transit photometry alone, unless a stellar mass-radius relation is assumed (Seager & Mallén-Ornelas 2003). We fix $M_\star = 1.0\ M_\odot$, based on the spectroscopic estimate by McCullough et al. (2006). Our results may be scaled to other choices for the stellar mass according to $R_\star \propto (M_\star/M_\odot)^{1/3}$ and $R_P \propto (M_\star/M_\odot)^{1/3}$. The planetary mass M_P is irrelevant to the model

[10] We assume a circular orbit because the radial velocity data show no evidence for a nonzero eccentricity, and in the absence of any evidence for additional bodies in the system, it is expected that tidal interactions have had sufficient time to circularize the orbit (see, e.g., Rasio et al. 1996; Trilling 2000; Dobbs-Dixon et al. 2004).

TABLE 2
System Parameters of XO-1

Parameter (1)	Median Value (2)	68% Confidence Limits	
		Lower (3)	Upper (4)
$R_\star$ ($R_\odot$)	0.928	−0.009[a]	+0.015[a]
		−0.013[b]	+0.018[b]
		−0.032[c]	+0.034[c]
R_P (R_J)	1.184	−0.014[a]	+0.025[b]
		−0.018[b]	+0.028[b]
		−0.042[c]	+0.047[c]
$R_P / R_\star$	0.13102	−0.00064	+0.00064
b	0.14	−0.10	+0.09
i (deg)	89.31	−0.53	+0.46
$t_{\rm IV} - t_{\rm I}$ (hr)	2.992	−0.015	+0.013
$t_{\rm II} - t_{\rm I}$ (minutes)	21.18	−0.47	+0.81
$u_1(z)$	0.128	−0.071	+0.061
$u_2(z)$	0.60	−0.14	+0.12
$2u_1(z) + u_2(z)$	0.858	−0.055	+0.049
$u_1(z) - 2u_2(z)$	−1.07	−0.34	+0.30
$T_c(17)$ (HJD)	2,453,875.92305	−0.00036	+0.00032
$T_c(18)$ (HJD)	2,453,879.8640	−0.0011	+0.0010
$T_c(19)$ (HJD)	2,453,883.80565	−0.00019	+0.00017
$T_c(20)$ (HJD)	2,453,887.74679	−0.00016	+0.00014

Notes.—The parameter values in col. (2) are the median values of the distributions shown in Fig. 3. The confidence limits in cols. (3) and (4) are based on the MCMC analysis.

[a] These uncertainties ignore the uncertainty in stellar mass. (For parameters with no designation, the uncertainty in the stellar mass is irrelevant.)

[b] These uncertainties include the 0.03 $M_\odot$ uncertainty in the stellar mass reported by McCullough et al. (2006) propagated according to $R_\star \propto (M_\star/M_\odot)^{1/3}$ and $R_P \propto (M_\star/M_\odot)^{1/3}$.

[c] These uncertainties include a stellar mass uncertainty of 0.10 $M_\odot$.

except for its minuscule effect on the relation between P and the semimajor axis; for completeness, we assume $M_P = 0.9M_J$, again following McCullough et al. (2006).

In total, there are nine free parameters describing 1309 photometric data points. The free parameters are $R_\star$, R_P, and i; the z-band limb-darkening parameters u_1 and u_2; and the four values of T_c. In practice, we found it better to fit for the parameters $2u_1 + u_2$ and $u_1 - 2u_2$, because the resulting uncertainties in those parameters are uncorrelated (as is shown below). We allowed the limb-darkening parameters to range only over the values that produce a monotonically decreasing intensity from the center of the star to the limb.

Prior to fitting the full set of observations, we fitted each of the six time series separately and determined the minimum χ^2 in each case. The resulting values of χ^2 per degree of freedom were 2.03 (FLWO 1.2 m, night 1), 1.39 (FLWO 1.2 m, night 2), 1.53 (Palomar 1.5 m), 0.25 (TopHAT, night 1), 0.50 (TopHAT, night 2), and 0.34 (TopHAT, night 3). Thus, it seems that the calculated uncertainties were somewhat underestimated for the FLWO and Palomar data, and overestimated for the TopHAT data. Before proceeding, we scaled the estimated uncertainties of each time series individually so that the resulting value of χ^2 per degree of freedom was unity. Table 2 gives the uncertainties *after* this scaling was performed.

We determined the best-fitting model using the AMOEBA algorithm (Press et al. 1992) to minimize the error statistic

$$\chi^2 = \sum_{j=1}^{1309} \left[\frac{f_j(\mathrm{obs}) - f_j(\mathrm{calc})}{\sigma_j} \right]^2, \qquad (2)$$
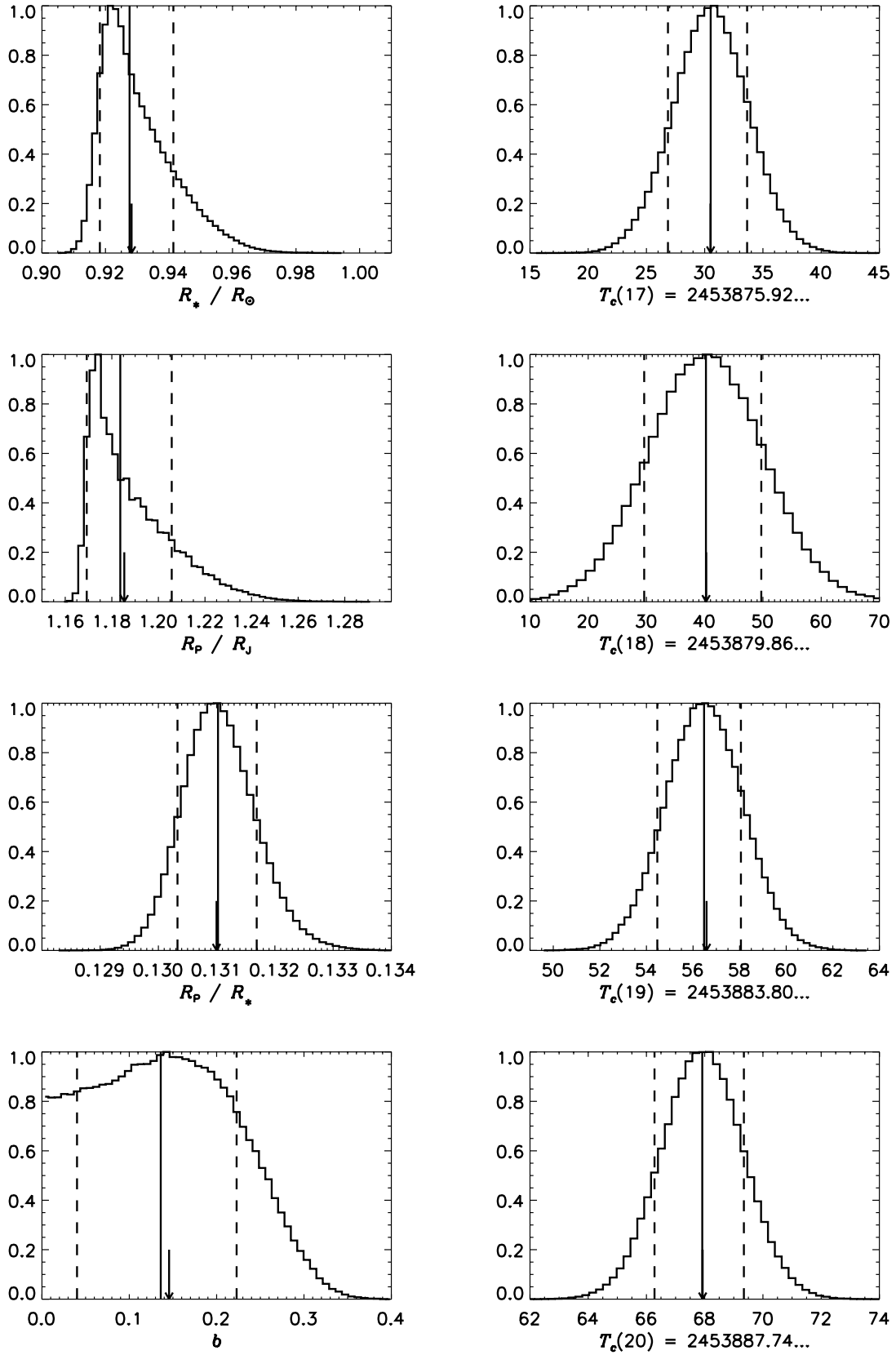
Fig. 3.—Estimated probability distributions of some planetary, stellar, and orbital parameters. The histograms show the results of 10 Markov chain Monte Carlo simulations, each with 400,000 points. The median of each distribution is indicated with a solid line. The dashed lines enclose 68% of the results, with equal probability on either side of the median. The arrows show the choice of parameters that minimizes χ^2. The numbers in Table 2 are the median values, with confidence limits given by the dashed lines.
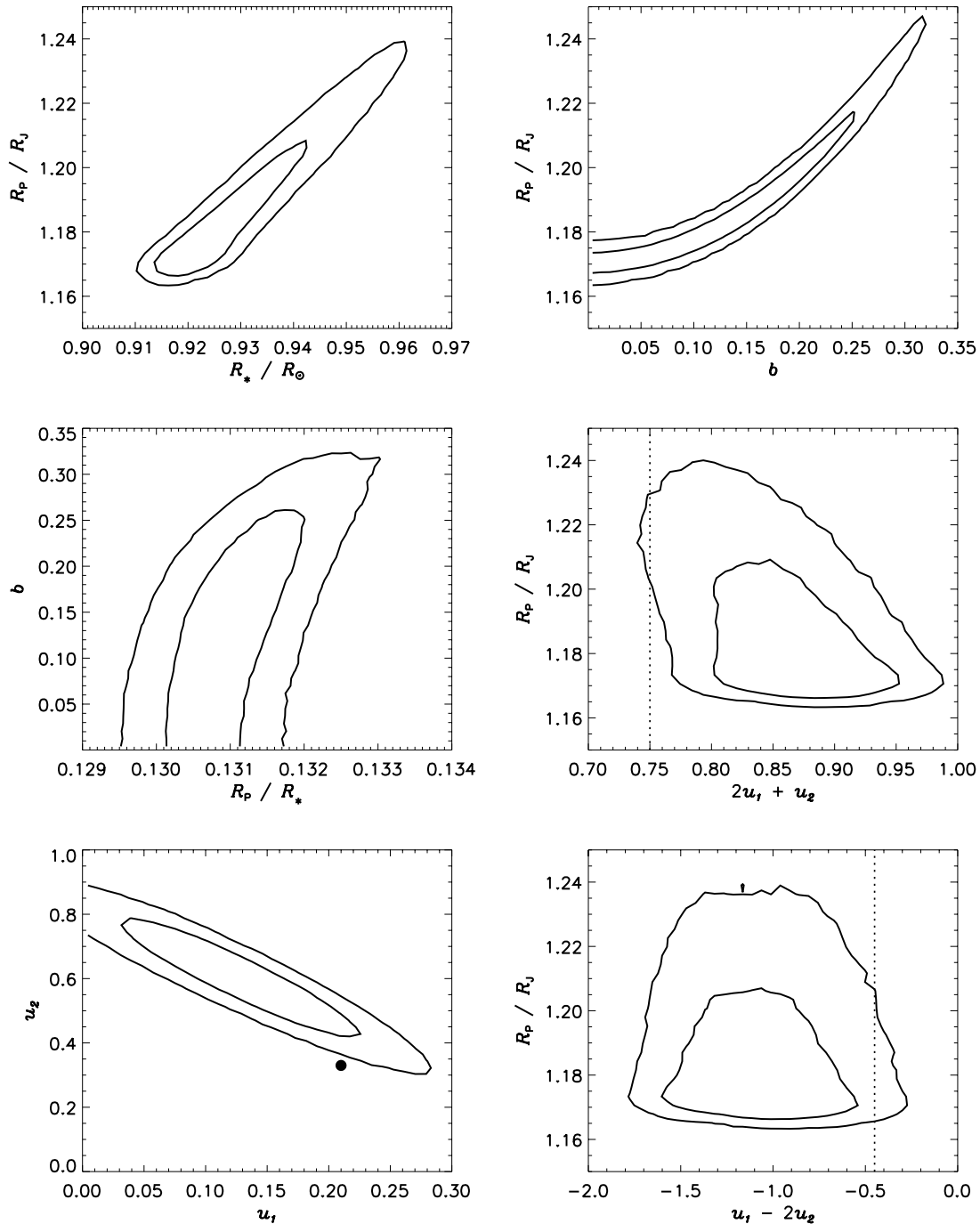
Fig. 4.—Joint probability distributions of some planetary, stellar, orbital, and limb-darkening parameters, based on the MCMC simulations. The contours are isoprobability contours enclosing 68% and 95% of the points in the Markov chains. In the u_1-u_2 plot, the filled circle shows the values calculated by Claret (2004). In the other plots involving limb darkening, the dotted lines show the values calculated by Claret (2004).

where $f_j(\mathrm{obs})$ is the flux observed at time t_j, σ_j is the corresponding uncertainty, and $f_j(\mathrm{calc})$ is the calculated value. In Figures 1 and 2, the left-hand panels show the best-fitting model as a solid line, and the right-hand panels show the results of subtracting the calculated values from the observed values. The FLWO z-band data show random-looking residuals with a standard deviation of 0.15% for the first night, and 0.12% for the second night. Almost all of the leverage on the stellar and planetary parameters comes from these data. The P60 data also show nearly random residuals, but at a higher level of 0.2%, and with occasional outliers. The TopHAT data are noisier, with a

standard deviation of 0.3%, and show some signs of correlated residuals (i.e., systematic errors). The uncertainties in the fitted parameters were estimated using two different methods, described below.

The first method was a bootstrap analysis, similar to those we have performed previously for the transiting exoplanets HD 209458b (Winn et al. 2005), OGLE-TR-10 (Holman et al. 2005), and HD 149026b (Charbonneau et al. 2006b). We refitted the parameters to each of 10^4 different "realizations" of the data. These realizations were sets of 1309 data points drawn randomly from the actual data set, with duplications allowed (i.e., with

replacement). Each realization was required to preserve the total number of points in each of the six individual time series. The resulting collection of 10^4 optimized parameter sets was taken to be the joint probability distribution for the parameters.

The second method was a Markov chain Monte Carlo (MCMC) simulation. In this method (described lucidly for astrophysicists by Tegmark et al. [2004] and Ford [2005]), a stochastic process is used to create a sequence of points in parameter space that approximates the desired probability distribution. The sequence, or "chain," is generated from an initial point by iterating a "jump function." In our case, the jump function was the addition of a Gaussian random number to each parameter value. If the new point has a lower χ^2 than the previous point, the jump is executed; if not, the jump is only executed with probability $\exp(-\Delta\chi^2/2)$. Under fairly benign mathematical assumptions, the chain will eventually converge to the desired probability distribution. To speed convergence, the Gaussian perturbations should be large, but not so large that all jumps are rejected. We set the relative sizes of the perturbations using the 1 σ uncertainties estimated previously by the bootstrap method, and we set the overall jump size by requiring that $\sim$25% of jumps are executed. We created 10 independent chains, each from a random initial position $\sim$5 σ away from the optimized parameter values. Each chain had 500,000 points, the first 20% of which were discarded to minimize the effect of the initial condition. The typical correlation length for each parameter (see Tegmark et al. 2004) was $\sim$400 points, giving an effective length of $\sim$1000 per chain. To check the convergence and the consistency between chains, we computed the Gelman & Rubin (1992) statistic for each parameter, which is a comparison between the interchain variance and the intrachain variance. The results were within a few percent of unity, a sign of good mixing and convergence.

The two methods produced very similar results. We also checked the results for the planetary and stellar radii using the more traditional approach of stepping each parameter through a sequence of values while allowing all of the other parameters to float, and identifying the values for which $\Delta\chi^2 = 1$ as the 68% confidence limits (as done by Brown et al. [2001], among others). Again, the values and the uncertainties were comparable to the results of the MCMC and bootstrap methods. For brevity, we report only the MCMC results for the remainder of this paper. The probability distributions for some of the parameters are shown in Figure 3, and some of the correlations between the parameters are shown in Figure 4. Table 2 lists the median value of each parameter with their 68% confidence limits, based on the MCMC results.

4. SUMMARY AND DISCUSSION

Through observations of four consecutive transits, we have significantly improved on the estimates of the system parameters of XO-1. The most interesting parameters are the radius of the star, the radius of the planet, and the midtransit times, which are discussed below. The results for the other parameters are not especially interesting but they do seem reasonable. The results for the orbital inclination are best described as an upper bound on the impact parameter b, which is the minimum projected star-planet distance, in units of the stellar radius. It is given by $b = a\cos i/R_\star$, where a is the orbital distance. The data favor a central transit, with $b < 0.27$ and $i > 88\overset{\circ}{.}53$ at the 95% confidence level.

Although the survey and follow-up photometry of McCullough et al. (2006) were impressive and built a convincing case for an exoplanet, those authors did not attempt to fit for the stellar radius when modeling the transit light curve. Instead, they used the value $R_\star/R_\odot = 1.00 \pm 0.08$, based on an interpretation of the stellar spectrum. This is because the inference of $R_\star$ from a transit light curve requires that the ingress and egress are well sampled and measured with a high signal-to-noise ratio. This type of data was not available. The higher precision and finer time sampling of our data, and of the z-band data in particular, allow for the determination of $R_\star$ from the light curve, without relying on spectral modeling and theoretical isochrones. The resulting "photometric" value of $R_\star$ is still subject to a systematic error due to the covariance with $M_\star$, but the dependence is fairly weak, $R_\star \propto M_\star^{1/3}$, generally leading to a smaller uncertainty in $R_\star$ than can be achieved from spectral modeling and theoretical isochrones.

Our result is $R_\star/R_\odot = 0.928^{+0.018}_{-0.013}$, which is consistent with (but more precise than) the value determined by McCullough et al. (2006). Here we have incorporated the 0.03 $M_\odot$ uncertainty in $M_\star$ determined by McCullough et al. (2006). We note that this radius is somewhat small for the G1 V spectral type of XO-1, but it is still consistent, given the stated uncertainties. We remind the reader again that the quoted result assumes $M_\star = 1.0~M_\odot$ and that the inferred $R_\star$ scales as $(M_\star/M_\odot)^{1/3}$. From the Yonsei-Yale isochrones, a stellar mass of $M_\star = 0.96~M_\odot$ corresponds to a radius of $R_\star = 0.91~R_\odot$ for solar metallicity and an arbitrary age of 3.6 Gyr (Yi et al. 2001). Thus, a 1.3 σ change in the assumed stellar mass would cause the stellar radius that is derived from the photometry to be precisely in line with theoretical expectations. We also note that the stellar radius uncertainty is a factor of 2–3 larger if a more conservative uncertainty of 0.10 $M_\odot$ is assumed for the stellar mass, as shown in Table 2.

Our derived radius of XO-1b is $R_P/R_J = 1.184^{+0.028}_{-0.018}$ (again assuming the uncertainty in the stellar mass to be 0.03 $M_\odot$). Previously, McCullough et al. (2006) found $R_P/R_J = 1.30 \pm 0.11$. These figures are also in agreement right within their respective 68% confidence limits. It is interesting to note that we obtain very precise agreement with McCullough et al. (2006) for all parameters if we first time-average our data into 5 minute bins (i.e., by a factor of 8, for the z-band data). The McCullough et al. (2006) data were averaged into bins ranging in width from 3 to 9 minutes, depending on the telescope used. We suggest that it is possible that some of the previous results were slightly biased by the coarser time sampling of the photometry. Resolving the degeneracy among the stellar radius, planetary radius, and orbital inclination requires adequate sampling of ingress and egress.

The uncertainties in the limb-darkening parameters u_1 and u_2 are highly correlated, with the linear combination $2u_1 + u_2$ being well constrained by the data, and the orthogonal combination $u_1 - 2u_2$ being weakly constrained by the data (Fig. 3, *bottom left panel*). We find $2u_1 + u_2 = 0.86 \pm 0.05$. This is 2 σ larger than the value based on the theoretical calculations of Claret (2004), which predict $u_1 = 0.21$, $u_2 = 0.33$, and $2u_1 + u_2 = 0.75$ (for the standard z band, $T = 5750$ K, $\log g = 4.5$, [M/H] = 0.05, and microturbulent velocity $v_t = 2.0$ km s^{-1}). The theoretical values are shown in Figure 4 as the filled circle in the u_1-u_2 plot, and as dotted lines in the other two limb-darkening plots. One might consider reducing the number of degrees of freedom and adopting the Claret (2004) values as fixed quantities. When we do so, we find $R_\star/R_\odot = 0.94$, $R_P/R_J = 1.22$, and $b = 0.26$ ($i = 88\overset{\circ}{.}65$), with the minimum χ^2 increased by 9. However, given the quality of the z-band data, the unknown level of uncertainty in the theoretical values, and the possible

differences between the FLWO 48 inch KeplerCam z band and the standard SDSS z band, we believe that fitting for the limb-darkening coefficients is more appropriate.

Some of the probability distributions shown in Figure 3 are asymmetric. This is typical of all fits to transit light-curve data. The fact that the orbital inclination has a maximum value (namely, $90°$), combined with the measured durations of the ingress, egress, and the full transit, imposes this asymmetry among the covariant parameters $R_\star$, R_P, and b.

Our downward revision of the planetary radius translates into an increased value for the mean density, 0.67 ± 0.07 g cm^{-3}. This value is 45%–56% that of Jupiter. This is comparable to, but less than, the mean densities of TrES-1 (0.84 g cm^{-3}; Sozzetti et al. 2004) and HD 189733b (0.93 g cm^{-3}; Bakos et al. 2006). For XO-1b's estimated equilibrium temperature $T_{eq} = 1100$ K (assuming Bond albedo $A_B = 0.4$ and our derived value of the stellar radius $R_\star = 0.928 \, R_\odot$) and its mass $M_P = 0.9 M_J$, the models of Bodenheimer et al. (2003) predict planetary radii of $R_P = 1.04 R_J$ and $1.11 R_J$ for models with and without a 20 $M_\oplus$ core, respectively. Our estimate of the radius of XO-1b is 2 σ larger than its predicted value, even for a planet without a core. HD 189733b's measured radius $R_P = (1.154 \pm 0.032) R_J$ (Bakos et al. 2006) is also larger than its theoretical value ($R_P = 1.03 R_J$ with a core; $R_P = 1.11 R_J$ without a core), given its equilibrium temperature $T_{eq} = 1050$ K and mass $M_P = (0.82 \pm 0.03) M_J$ (Bouchy et al. 2005). In contrast, Laughlin et al. (2005) showed that TrES-1's measured radius $R_P = (1.08 \pm 0.05) R_J$ (Laughlin et al. 2005) is consistent with its theoretically predicted value ($R_P = 1.05 R_J$ with a core; $R_P = 1.09 R_J$ without a core).

The measured radii of both XO-1b and HD 189733 are consistent with the predictions of Bodenheimer et al. (2003) if "kinetic heating" is included. In these models, $\sim 2\%$ of the stellar insolation is deposited at depth, following the work of Guillot & Showman (2002). However, as pointed out by Burrows et al. (2003), the measured radius of a transiting planet refers to the scale height of the planetary atmosphere at which the stellar flux encounters optical depth ~ 1 in the direction toward the observer. This radius can be larger than the values calculated by Bodenheimer et al. (2003), which refer to the radius of the Rosseland mean photosphere. If this effect is taken into account, the theoretical models are in better agreement with the measured radii of transiting planets, although they still have difficulty with the case of HD 209458b (which has a mean density of 0.36 g cm^{-3}, as estimated most recently by Knutson et al. 2006). The age of XO-1 is also uncertain; the expected size of the planet would be larger if the system were younger (Burrows et al. 2003). Whether an extra source of heat is required to account for the mean density of XO-1b, as seems to be the case for HD 209458b, is an important topic for future theoretical work. The kinetic heating model, proposed to explain the apparent inflation of HD 209458b, would naturally predict that many other hot Jupiters should be inflated. Other explanations, such as ongoing tidal circularization due to an eccentricity exchange with a third body (Bodenheimer et al. 2001), or the trapping in a Cassini state with nonzero obliquity (Winn & Holman 2005), would
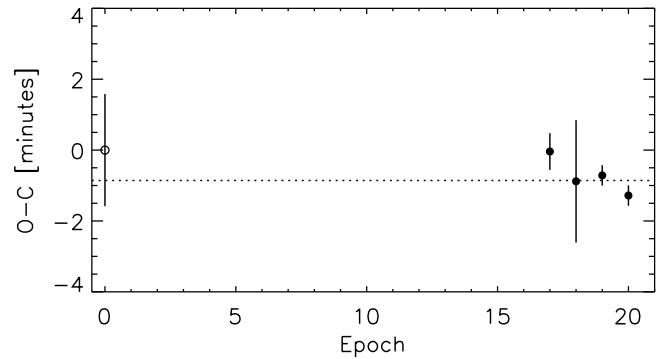

Fig. 5.—Timing residuals for the four observed transits, according to the ephemeris of McCullough et al. (2006; see also eq. [1]). The first point corresponds to the T_c of McCullough et al. (2006). The points lie on a horizontal line, and therefore the data are marginally consistent with a constant period.

seemingly have difficulty accounting for a large population of inflated objects.

The accuracy of our transit times ranges from 0.2 minutes for the FLWO z-band observations to 2.5 minutes for the transit observed solely by TopHAT. Figure 5 shows the differences between the observed and predicted times of midtransit, as a function of transit epoch. The predicted times assume the average orbital period determined by McCullough et al. (2006) and a reference time based on our observations. So far, all the times are marginally consistent with a constant period. These observations provide accurate anchors for future searches for transit time variations.

REFERENCES

Agol, E., Steffen, J., Sari, R., & Clarkson, W. 2005, MNRAS, 359, 567
Bakos, G., Noyes, R. W., Kovács, G., Stanek, K. Z., Sasselov, D. D., & Domsa, I. 2004, PASP, 116, 266
Bakos, G. A., et al. 2006, ApJ, 650, 1160
Bodenheimer, P., Laughlin, G., & Lin, D. N. C. 2003, ApJ, 592, 555
Bodenheimer, P., Lin, D. N. C., & Mardling, R. A. 2001, ApJ, 548, 466
Borucki, W. J., et al. 2003, in ASP Conf. Ser. 294, Scientific Frontiers in Research on Extrasolar Planets, ed. D. Deming & S. Seager (San Francisco: ASP), 427

Bouchy, F., et al. 2005, A&A, 444, L15
Brown, T. M., Charbonneau, D., Gilliland, R. L., Noyes, R. W., & Burrows, A. 2001, ApJ, 552, 699
Burrows, A., Sudarsky, D., & Hubbard, W. B. 2003, ApJ, 594, 545
Charbonneau, D., Brown, T. M., Burrows, A., & Laughlin, G. 2006a, in Protostars & Planets V, ed. B. Reipurth, D. Jewitt, & K. Keil (Tucson: Univ. Arizona Press), in press (astro-ph/0603376)
Charbonneau, D., et al. 2006b, ApJ, 636, 445

Claret, A. 2000, A&A, 363, 1081
———. 2004, A&A, 428, 1001
Dobbs-Dixon, I., Lin, D. N. C., & Mardling, R. A. 2004, ApJ, 610, 464
Dravins, D., Lindegren, L., Mezey, E., & Young, A. T. 1998, PASP, 110, 610
Ford, E. B. 2005, AJ, 129, 1706
Gelman, A., & Rubin, D. B. 1992, Stat. Sci., 7, 457
Guillot, T., & Showman, A. P. 2002, A&A, 385, 156
Holman, M. J., & Murray, N. W. 2005, Science, 307, 1288
Holman, M. J., Winn, J. N., Stanek, K. Z., Torres, G., Sasselov, D. D., Allen, R. L., & Fraser, W. 2005, ApJ, submitted (astro-ph/0506569)
Knutson, H., Charbonneau, D., Noyes, R. W., Brown, T. M., & Gilliland, R. L. 2006, ApJ, submitted (astro-ph/0603542)
Laughlin, G., Wolf, A., Vanmunster, T., Bodenheimer, P., Fischer, D., Marcy, G., Butler, P., & Vogt, S. 2005, ApJ, 621, 1072

Mandel, K., & Agol, E. 2002, ApJ, 580, L171
McCullough, P. R., et al. 2006, ApJ, 648, 1228
Press, W. H., Teukolsky, S. A., Vetterling, W. T., & Flannery, B. P. 1992, Numerical Recipes in C (2nd ed.; Cambridge: Cambridge Univ. Press)
Rasio, F. A., Tout, C. A., Lubow, S. H., & Livio, M. 1996, ApJ, 470, 1187
Seager, S., & Mallén-Ornelas, G. 2003, ApJ, 585, 1038
Sozzetti, A., et al. 2004, ApJ, 616, L167
Tegmark, M., et al. 2004, Phys. Rev. D, 69, 103501
Trilling, D. E. 2000, ApJ, 537, L61
Winn, J. N., & Holman, M. J. 2005, ApJ, 628, L159
Winn, J. N., et al. 2005, ApJ, 631, 1215
Yi, S., Demarque, P., Kim, Y.-C., Lee, Y.-W., Ree, C. H., Lejeune, T., & Barnes, S. 2001, ApJS, 136, 417
Young, A. T. 1967, AJ, 72, 747